Author/s:
Knapp, EM;Dagastine, RR;Tu, RS;Kretzschmar, I

Title:
Effect of Orientation and Wetting Properties on the Behavior of Janus Particles at the Air-Water Interface.

Date:
2020-01-29

Citation:
Knapp, E. M., Dagastine, R. R., Tu, R. S. & Kretzschmar, I. (2020). Effect of Orientation and Wetting Properties on the Behavior of Janus Particles at the Air-Water Interface.. ACS Applied Materials and Interfaces, 12 (4), pp.5128-5135. https://doi.org/10.1021/acsami.9b21067.

Effect of Orientation and Wetting Properties on the Behavior of Janus Particles at the Air-Water Interface

Ellen M. Knapp[1,2], Raymond R. Dagastine[2], Raymond S. Tu[1] and Ilona Kretzschmar[1*]*

[1] Department of Chemical Engineering, The City College of New York, New York, 10031, United States

[2] Department of Chemical Engineering and the Particulate Fluids Processing Centre, University of Melbourne, Parkville, 3010, Australia.

**Corresponding Authors: kretzschmar@ccny.cuny.edu, rrd@unimelb.edu.au*

ABSTRACT

The adhesion force and contact angle of gold-capped silica Janus particles and plain silica particles at an air-water interface are studied via colloidal atomic force microscopy. Particles are attached to cantilevers at various orientations and wetting properties of the gold surface are varied through modification with dodecanethiol. Thiol modification increases the hydrophobicity of the gold surface thereby increasing the difference between the contact angles of the gold hemisphere and the silica hemisphere and, thus, increasing the degree of amphiphilicity of the Janus particle.

Subsequently, the colloidal probe is pushed into a stationary bubble from the water phase followed by retraction into the water phase. Adhesion force is found to be higher for Janus particles than isotropic silica particles, regardless of orientation of the anisotropic hemisphere. Particles with their polar half oriented towards the water and apolar half facing the air shows an increase in adhesion force and contact angle as the degree of amphiphilicity of the particles increases. For particles of the reverse orientation, no significant difference is observed as wetting properties change. Both adhesion force and contact angle display an inverse relationship with cap angle for particles with a higher degree of amphiphilicity. These results are of importance for using Janus particles to stabilize interfaces as well as for understanding the equilibrium height of Janus particles at the interface, which will impact capillary interactions and thus self-assembly.

KEYWORDS Amphiphilic Janus particles, Colloidal Atomic Force Microscopy, Interfacial stability, Interfacial assembly.

Anisotropic Janus particles, consisting of two chemically distinct hemispheres, have shown promise to improve technologies in the fields of emulsions and foams[1,2], pharmaceuticals[3,4], and catalysis[5]. One unique feature of Janus particles is the ability to tune the wetting properties in order to achieve desired behavior, such as packing and patterning, at an interface. The ability to control the patterning of particles has many applications, one being films with tunable optical properties. In nature, many species, such as the Male Eastern Bluebird[6] and blue spikemoss[7], exhibit structural color, which arises from quasi-periodic nanostructures. Self-assembly of particles at an interface presents the opportunity to generate quasi-ordered nanostructures in a bottom up fashion. Furthermore, packed particle layers with periodicity close to the wavelength of light can exhibit unique optical properties.[8–11] Janus particles provide additional variables, such as wetting properties and orientation, which can be tuned to allow for greater control over particle self-assembly and packing behavior at the interface.

There is a wide body of literature describing Janus particles at interfaces [12–19]. Many simulations and theoretical works explore the role amphiphilicity plays in influencing the energy landscape of Janus particles at an interface.[15,16,20–23]Previous studies[15,16,23,24]have indicated the presence of a deep energy well when in the so called Janus-preferred orientation, where the interface lies at the Janus boundary, the apolar hemisphere is entirely in the apolar phase, and vice versa. In past experiments, Janus particles have been observed to take on energetically unfavorable configurations at the interface[12,25] (i.e., with their polar half in an apolar solvent) and it has been hypothesized that the contact line around a Janus particle may undulate, resulting in quadrupolar capillary interactions and thus attraction between particles.[12] Looking at particles in energetically unfavorable orientations in addition to the expected configuration, provides insight into the influence of orientation of the Janus boundary on particle position and assembly at the interface.

The fundamental understanding of the impact of colloid orientation and amphiphilicity is critical to advancing the field of self-assembly of Janus particles at an interface.

Quantifying the relative stability of the particles at the interface is important to processability. Adhesion force gives a direct measure of how much force it takes to remove a particle from the interface, and thus, is tied to interfacial stability. Additionally, measurements of advancing and receding contact angle provide insight into the contact line behavior averaged around a single Janus particle as well as the equilibrium height of the particles at the interface. The Janus particles used in the experiments discussed here are synthesized through evaporative methods, a widely used synthesis technique that can be used to make quantities of Janus particles on the scale needed for self-assembly.[17,26] For applications in interfacial assembly, the contact line around a Janus particle and the subsequent capillary interactions between particles represent a major driving force that can be used to generate ordered structures.

One way to directly measure the behavior of individual particles at interfaces is through colloidal probe atomic force microscopy (colloidal AFM).[27] Colloidal AFM differs from traditional AFM in that instead of using a prefabricated AFM tip, one attaches a colloid to an AFM cantilever. Through direct force measurements, the interactions between the colloid and a substrate or the colloid and an interface can be quantified.[28] For the experiments reported here, force measurements are taken as Janus particles of various orientations attached to a cantilever (**Fig. 1A1-3**) and immersed in an aqueous phase are pushed into an air bubble (**Fig. 1B**). Colloidal AFM at the air-water interface allows measuring particle stability through the quantification of adhesion force[29] and contact angle of an individual particle[30]. The jump in distance, D_r is defined by the point at which the force returns to zero after the particle has contacted the interface and is equivalent to the

equilibrium height of the particle. From this point, the receding contact angle, θ_r, can be determined:

$$\cos(\theta_r) = \frac{(R - D_r)}{R} \qquad \text{Eq. 1}$$

Where R = particle radius and D_r = receding jump in distance. Eq. 1 is the same for advancing contact angle, θ_a, but instead of D_r, D_a is used. Here, receding and advancing refer to the motion of the water phase over the surface of the particle[30–32]; for example, receding jump in distance and contact angle are measured as the cantilever is approaching the bubble because the water is *receding* over the surface of the particle as it passes through the air-water interface. When probing a bubble, a pair of force curves is obtained, that is the approach curve (red) and the retract curve (blue) as shown in **Figure 1C**. Additional force curve examples for all particle types are provided in the Supporting Information (**Fig. S1**).

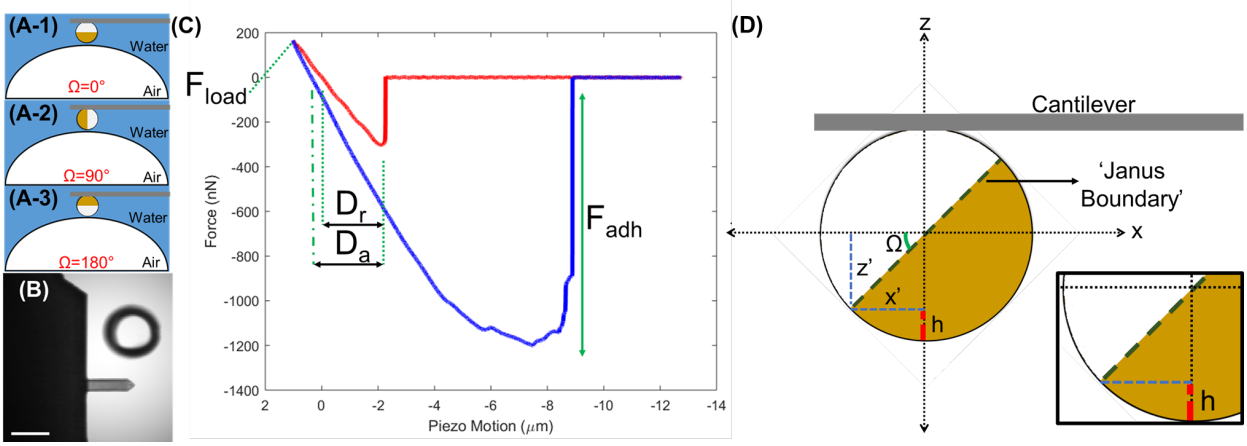

Figure 1: Experimental details for Colloidal AFM. (A 1-3) – Schematic of a Janus particle attached to a cantilever at various orientations probing a bubble. (B) Image from the inverted microscope coupled to the AFM showing the cantilever with a particle attached above the bubble. Scale bar is 100 μm. (C) Example force curve showing parameters used in the analysis. Here, F_{load} is loading force (N), F_{adh} is adhesion force (N), D_r and D_a represent receding and advancing jump-in distance (μm), respectively and are used to calculate advancing and receding contact angles according to Eq. 1. (D). Schematic illustrating the Janus boundary height, h, and cap angle, Ω. Inset zooms in on h for clarity.

Colloidal AFM has been used to study particles with a variety of wetting properties[31–33]. Recent work has looked into the behavior of physically heterogeneous particles to better understand the effects of pinning[34,35]. For the pure pinning case, Ally et al. report that the jump in distance matches the height of the pinning site and that the measured adhesion force exceeds that which is predicted if the contact line is sliding. Instead, adhesion force can be modelled using contact angle limits as defined by the Gibbs inequality, rather than assuming a constant contact angle [34]. In the case of rough colloids with multiple pinning sites, adhesion force varies with loading force and the detachment of the colloid from the interface is more abrupt than that of a smooth particle with a sliding contact line [35].

Janus particles present the opportunity to study another class of contact line behavior. The Janus boundary is chemically heterogeneous but not necessarily physically rough. Recent work has shown that for Janus particles synthesized through evaporative methods, the thickness of the cap decreases close to the equator of the particle and therefore the transition from one hemisphere to the other is relatively smooth.[36] Colloidal AFM measurements on Janus particles reported here are the first to be done on chemically anisotropic colloids.

In this work, 8 μm gold-capped silica Janus particles are attached to AFM cantilevers with different orientations and pushed through the air-water interface of a stationary bubble while taking direct force measurements. From these measurements, the adhesion force as well as the advancing and receding contact angles are calculated (see **Fig. 1C** and Eq. 1). Janus particle orientation is characterized via He-Ion microscopy (HIM), enabling the measurement of both cap angle (Ω) and height to the Janus boundary (h) (see **Fig. 1D**) without the need of additional coatings common to scanning electron microscopy. Measurements are taken on both unmodified and dodecanethiol-

modified Janus particles to study the impact of increasing the degree of amphiphilicity of the particle.

Knowing that Janus particles can take on random orientations at the interface, we seek to understand differences between the adhesion force and contact angle of Janus particles at various orientations and how they might influence assembly. Furthermore, the amphiphilic nature of Janus particles gives an additional variable through which self-assembly can be controlled. Understanding how the difference in wetting properties between the two hemispheres influences particle stability and equilibrium height at the interface is critical in the utilization of amphiphilicity to achieve prescribed interfacial behavior.

EXPERIMENTAL METHODS

Janus Particle Synthesis: Gold-capped silica Janus particles are synthesized via physical vapor deposition (PVD). Evaporative assembly[37] is used to make monolayers of 8 μm silica particles (Fiber Optics Center) on glass slides. Monolayers are placed inside a PVD machine (Cressington Coating System, Ted Pella), the machine is pumped to pressures below 10^{-6} mbar, and then the metal is evaporated onto the particle layers. For these experiments, particles are capped with 5 nm of titanium as an adhesion layer followed by 10 nm of gold (Ted Pella).

Attachment of Colloids to AFM Cantilevers: Anisotropic particles are attached to AFM cantilevers (All-In-One Tipless Probes, BudgetSensors) using UV-curable adhesive (Norland Optical Adhesive 61, Norland Products Incorporated). Following attachment, particles are cured using a 100 W mercury lamp for ten minutes. The glue is allowed to age either by waiting one week before experiments or baking for 12 hours at 50°C in order to achieve its maximum strength.

Characterization of Particle Orientation: He-Ion microscopy (HIM) is used to image the particles on the cantilevers, in order to characterize their orientation. Unlike more traditional scanning electron microscopes, the HIM system is charge compensated, allowing for high resolution imaging without additional coatings on the sample. Owing to its higher electron density, the gold hemisphere appears brighter than the silica hemisphere in HIM images, allowing for the position of the Janus boundary to be discerned. Images are taken from the top-down, from the side, and from several different angles in order to fully characterize the location of the Janus boundary (see **Fig. 2**). From the HIM images, cap angle, Ω, and distance from the top of the particle to the Janus boundary, h, are determined, as shown in **Figure 1D**. The cap angle is defined as the angle between the Janus boundary and the x-axis, which is drawn parallel to the cantilever and passed through the midpoint of the Janus boundary. With this definition, $\Omega = 0°$ corresponds to a Janus particle with the gold half facing the bubble and the silica half facing the cantilever, $\Omega = 90°$ is Janus particle on its side, and $\Omega = 180°$ describes a Janus particle where silica is facing the bubble and the gold hemisphere points towards the cantilever. Particles found to have an excess of glue are excluded from analysis. Examples showing an acceptably attached particle that is included in the data set versus a cantilever with excess glue that is rejected from analysis can be found in the Supporting Information (**Fig. S2**).

Characterization of Particle Surface Roughness: After the measurements are completed, reverse imaging of the cantilevers is performed in order to quantify surface roughness. The roughness is determined by dragging the cantilever in contact mode over a 20 μm square of a spiked grating (TGT1, NT-MDT Spectrum Instruments, Russia). Because the grating is sharper than the cantilever tip (i.e., the particle), the imaging yields a picture of the particle instead of the sample. By flattening the image, one can measure the roughness of the particle surface.[38] Values for surface

roughness averaged over the particle surface facing the bubble range from 0.5 to 7 nm (see Supporting Information, **Fig. S3**).

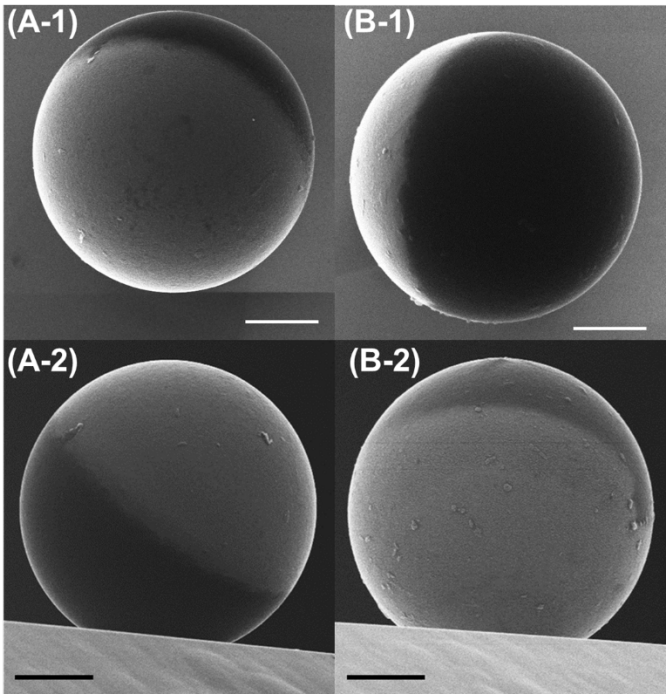

Figure 2: HIM images of AFM cantilevers 4 and 9. (A-1) Top view of cantilever 4 as captured by HIM. Here h = 1.1 μm and Ω = 44°. (A-2) Side view of cantilever 4. (B-1) Top view of cantilever 9. Here h = 1.3 μm and Ω = 138°. (B-2) Side view of cantilever 9. All scale bars are 2 μm.

Thiolization of the Gold Surface: Wetting properties of the particles are varied through modification of particles with dodecanethiol after attachment, which increases the hydrophobicity of the gold surface. Thiolization is carried out by soaking the cantilevers in a 10mM ethanolic thiol solution for 24 hours followed by rinsing with ethanol and then deionized water. Planar contact angles for each of the surfaces are measured using the sessile drop technique (Attension Theta Tensiometer, Biolin Scientific). Silica, C0 gold and C12 gold are found to have contact angles of <10°, 69°, and 112°, respectively, (see Supporting Information, **Table S1**). The same cantilevers are run unmodified (C0) and dodecanethiol modified (C12). Therefore, particle orientation, Ω, is fixed while the degree of amphiphilicity of the particles is increased.

Force Measurements at the air-water Interface: Force measurements are taken on an Asylum MFP-3D Atomic Force Microscope (Asylum Research) as Janus particles are pushed into and then pulled out of the air-water interface of a stationary bubble. Bubbles are generated on the hydrophobic glass bottom of a fluid cell filled with deionized water. The glass is hydrophobized via esterification[39] by boiling the glass round in octanol overnight. All glassware involved in the experiments is cleaned in a three-step procedure involving washing with 10% Ajax detergent, then 10% sodium hydroxide solution, and finally 10% nitric acid. After each step, the glassware is rinsed with copious amounts of deionized water. Bubble generation is achieved either ultrasonically using a transducer (Undatim Ultrasonics D-Reactor) at a frequency of 515 kHz and a power of 25W, or via degassing, in which vacuum is pulled on the fluid cell and the lower pressure allowed for the formation of bubbles on the glass surface.[40] For each experiment, over 100 force curves are collected while loading force is varied. Initial approach and retract velocities are varied, and no dependence on the force data is observed from 200 nm/s to several microns/s. Thus, approach and retract velocity are held fixed at 2 μm/s in the experiments reported here. Values for jump in distance, advancing and receding contact angle, and adhesion force are extracted from each force curve and averaged for the experiment. The error shown is one standard deviation. Spring constants of the cantilevers are measured after experiments using the thermal method (Hutter and Bechhoefer method)[41] and ranged from 2 to 15 N/m.

Table 1. Cantilever's h value vs jump-in distance for the unmodified (C0) and dodecanethiol modified (C12) case. Shaded boxes indicate cases in which the jump in is greater than *h* and the Janus boundary comes into contact with the interface upon first contact. Contact surface indicates the particle surface (gold, silica) that will touch the air-water interface first, based on the orientation of the particle. The double black line marks the point at which particle orientation transitions from gold contacting the bubble first to gold/silica and then silica contacting the bubble first.

Cantilever	Ω (°)	h (μm)	Jump in Distance C0 (μm)	Jump in Distance C12 (μm)	Contact Surface
1	3	3.4	0.93 ± 0.33	3.93 ± 0.08	Au
2	3	1.5	1.02 ± 0.06	3.19 ± 0.10	Au
3	28	2.2	0.69 ± 0.91	2.13 ± 1.63	Au
4	42	2	1.55 ± 0.16	2.70 ± 0.04	Au
5	64	0.8	0.80 ± 0.07	2.38 ± 1.18	Au
6	90	0	0.71 ± 0.10	0.76 ± 0.12	Au/Si
7	100	0.1	0.38 ± 0.09	0.27 ± 0.09	Si
8	108	0.2	0.39 ± 0.78	0.10 ± 0.04	Si
9	125	0.7	1.04 ± 0.03	0.90 ± 0.95	Si
10	135	1.3	0.87 ± 0.05	0.09 ± 0.04	Si

RESULTS AND DISCUSSION

From the force curves, jump-in distances on the approach curve are tabulated and compared to the h values to determine cases in which the Janus boundary comes into contact with the air-water interface upon initial contact (see **Table 1**). We find that jump-in distance is equivalent to D_r (see **Fig 1C**). Jump-in distance is measured by taking the difference between the piezo position at first contact of the particle with the bubble, when the slope of the force curve becomes negative on the approach curve, and the piezo position at the point that force returns to zero on the approach, indicating the particle has reached its equilibrium height. From side-view HIM images of the particles, such as those shown in **Figure 2**, h is determined by measuring the distance between the top of the particle and the Janus boundary. For cases in which the Janus boundary is tilted, the

shortest distance to the Janus boundary is taken as h. **Table 1** shows that for almost all particles, the Janus boundary contacts the interface immediately, especially after thiol modification.

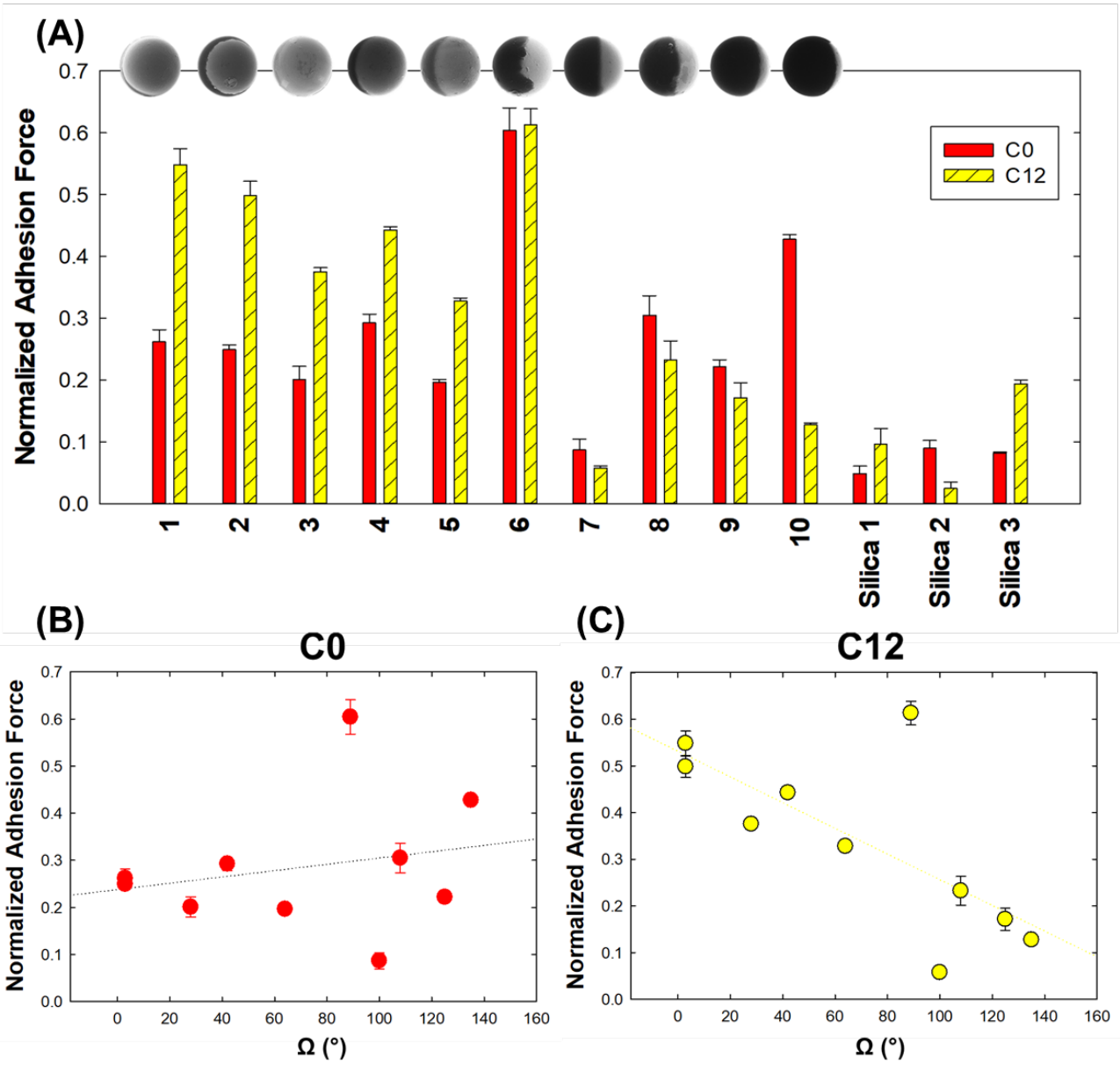

Figure 3: Adhesion fore vs contact angle, Ω. (A) Normalized adhesion force for cantilevers of various orientations. Top view HIM images of the cantilevers, i.e., particle surface touching the interface, are shown above the graph. (B) Normalized adhesion force vs Ω for unmodified cantilevers. (C) Normalized adhesion force vs Ω for dodecanethiol modified cantilevers. Lines show linear regression fit to guide the eye. Error bars represent one standard deviation from analysis of ~100 force curves.

Figure 3 shows the adhesion force normalized by the maximum possible capillary force, $2\pi\gamma R$, where γ is the interfacial tension and is taken to be 0.072 N/m. R is the particle radius and is measured for each particle from the HIM images. In **Figure 3A**, particles are ordered from the lowest to highest Ω values, as illustrated by the top-down HIM images overlaid on the chart. Data for the unmodified case (C0, shown in red) and the dodecanethiol modified case (C12, shown in yellow with black stripes) are displayed side-by-side for each cantilever in order to highlight the impact of the thiol modification.

Janus particles of all orientations, with the exception of cantilever 7 discussed below, display a higher adhesion force than isotropic silica particles, indicating that they are more interfacially stable than their isotropic counterparts, which is in agreement with theoretical prediction[20] and experimental observations[1]. As a control, silica particles are characterized in both their unmodified form and after the same thiolation protocol used for Janus particles. There is a small change in the adhesion force of the particles after modification, which is most likely due to contaminants from the ethanol or the thiol adsorbing to the silica surface (**Fig. 3A**, right most bars).

Figure 3B-C show adhesion force as a function of cap angle, Ω, for the unmodified, (see **Fig. 3B**), and dodecanethiol-modified case (see **Fig. 3C**). The degree of amphiphilicity of the particles impacts the relationship between Ω and adhesion force. For the C12 case, as the cap angle increases the adhesion force decreases. In contrast, for the C0 case, no trend is observed between the cap angle and adhesion force, which implies that as the degree of amphiphilicity increases, the effect of orientation also increases. The difference in behavior between the C0 and C12 case is in line with previous studies[20] on the energy landscape of a Janus particle at the interface where a greater difference between the wetting properties of the two hemispheres of the particles leads to a larger energy well for the case where the particle sits at the interface with its polar half in the

polar phase. The higher degree of amphiphilicity in the C12 case, leads to a larger adhesion force and, likewise, a greater difference in adhesion force between the energetically favorable orientation ($\Omega = 0°$) and the energetically unfavorable orientation ($\Omega = 180°$).

It is important to note an outlier to the trend of decreasing adhesion force at $\Omega = 90°$. The adhesion force for cantilever 6 is higher than expected in both the C0 and C12 case. As can be seen in **Figure 3A**, the particle has a cap defect along the Janus boundary, which faces the bubble and immediately interacts with the air-water interface upon contact. The defect increases the roughness of the surface and we hypothesize that the defect pins the interface, leading to high adhesion forces. The increase in adhesion force in the presence of a cap defect implies that the roughness of the Janus boundary is significant in influencing interfacial stability. Measurements of surface roughness (see Supporting Information, **Fig. S3**) support the hypothesis. Cantilever 6 has the highest surface roughness of all of the cantilevers analyzed.

Furthermore, the adhesion force of cantilever 7 is much lower than that of 6 or 8 and resembles that of unmodified silica. This cantilever has the lowest measured surface roughness across the entire data set and so it is not expected to have roughness-induced adhesion and may be indicative of purely wetting-influenced adhesion. We hypothesize that at intermediate orientations ($\Omega \sim 90°$), the interface is highly deformed and, thus, in a high-energy state. Our hypothesis is supported by work from Rezvantalab et al.,[42] who report the calculated interfacial adsorption difference for a 10 nm Janus particle for a deformed interface vs a flat interface is 1200kT. Therefore, when the cantilever retracts away from the bubble, the interface cannot sustain the deformation, resulting in low adhesion force. The study of intermediate Janus orientations represents an exciting prospect for future work.

Differences in adhesion forces between the C0 and C12 case vary with the position of the Janus boundary relative to the interface. For lower Ω values, adhesion force increases as one goes from C0 to C12. When $\Omega \geq 90°$, the difference in behavior between C0 and C12 is negligible or adhesion force decreases. This trend may be due to the fact that in cases where $\Omega \geq 90°$, as the interface comes into contact with the Janus boundary, it would have to deform substantially in order to assume the preferred contact angle with the gold hemisphere. Such deformations represent a high energy state and therefore the interface cannot achieve high contact angles and will not deform any further to hold onto the particle as it is pulled from the interface resulting in a low adhesion force.

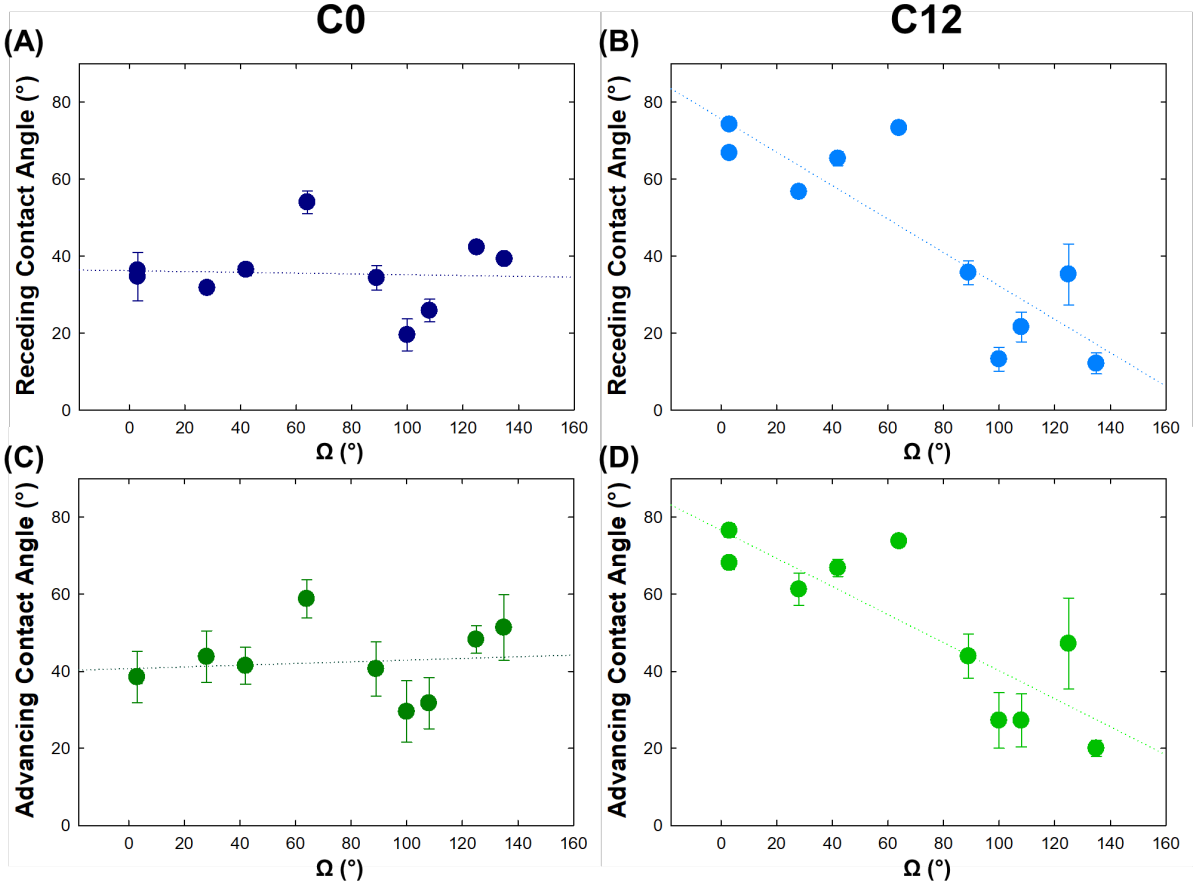

Figure 4: Contact Angle, θ, vs Cap Angle, Ω. (A) Receding Contact Angle, θ_r, vs Ω for unmodified gold. (B) Receding Contact Angle, θ_r, vs Ω for dodecanethiol modified gold. (C) Advancing Contact Angle, θ_a, vs Ω for unmodified gold. (D) Advancing Contact Angle, θ_a, vs Ω for dodecanethiol modified gold. Lines show linear regression fit to guide the eye. Error bars represent one standard deviation from analysis of ~100 force curves.

Contact angle measurements show similar results to adhesion force, as depicted in **Figure 4**. All Janus particles have a higher contact angle ($\theta > 20°$) when compared to isotropic silica ($\theta < 20°$). The higher contact angles indicate that Janus particles have a tendency to sit further in the air phase than in the water phase when compared to unmodified silica particles. Additionally, the contact angle decreases as cap angle increases for particles with a higher degree of amphiphilicity (see **Fig. 4C** and **D**), but in the unmodified gold case, no trend is observed (see **Fig. 4A** and **B**). It is important to note that macroscopic planar contact angle measurements and single particle contact angle measurements measured via colloidal AFM are known to differ.[30] The anomalous behavior in adhesion force seen at $\Omega = 90°$, is not present in the contact angle measurements, which implies that the rough cap defect does not impact equilibrium height of the particle and corroborates our proposed pinning mechanism where the interface becomes pinned on the defect while being pulled out of the bubble.

When one considers applications in interfacial self-assembly, these results represent an important contribution to the understanding of equilibrium height of Janus particles at an air-water interface and their overall stability. The average normalized adhesion force of an amphiphilic Janus particle with its hydrophobic cap in air and hydrophilic hemisphere in water ($F_{avg,C12\text{-}JP,\Omega<90°} = 0.44 \pm 0.09$) is more than four times that of an isotropic silica particle ($F_{avg,SiO2} = 0.09 \pm 0.06$), which is in good agreement with the findings of previous analytical work.[20] For energetically unfavorable orientations of Janus particles ($\Omega > 90°$), there is still an increase in the average normalized adhesion force compared to isotropic silica (more than a 50% increase for the C12 case, $F_{avg,C12\text{-}JP,\Omega>90°} = 0.18 \pm 0.05$, and the adhesion force is nearly double for the unmodified case,

$F_{avg,C0\text{-}JP,\,\Omega>90^\circ} = 0.32 \pm 0.1$). The higher adhesion force for Janus particles of all orientations but the $\Omega = 90^\circ$ orientation implies that the chemical heterogeneity of the particle surface gives it greater interfacial stability and represents the first time this stability has been demonstrated experimentally for a single Janus particle with a well-known orientation.

We have found that, for particles with a higher degree of amphiphilicity, orientation of the particle will determine its equilibrium height and that, in turn, will impact particle-particle interactions at the interface. When Janus particles with a high degree of amphiphilicity have their apolar half in air and their polar half in water, the contact angle approaches 90°, implying the equilibrium height is approximately at the equator of the particle. As Ω increases, i.e., the Janus boundary is less and less aligned with the interface and more of the apolar hemisphere is in contact with the water, the equilibrium height of the particle shifts such that it is at equilibrium when it is further into the water phase than the air phase. If amphiphilic particles of various orientations are placed at an interface together, the differences in heights between the particles will influence capillary interactions. For Janus particles with a lower degree of amphiphilicity, the contact angle never reaches 90°, even in the case where the hydrophobic cap is in air and the hydrophilic hemisphere is in water. For all orientations, the equilibrium height stays relatively constant. Capillary interactions between the particles could still arise from complex contact line behavior (undulations), but are not likely to be due to differences in height at the interface. Thus, for Janus particles, orientation at the interface is important in determining how they will self-assemble.

CONCLUSIONS

We have studied the behavior of micron sized Janus particles of various orientations and wetting properties using colloidal AFM. The experiments have allowed for direct measurement of adhesion

force and contact angle of individual particles with various orientations and wetting properties. Adhesion force is greater for Janus particles of all orientations when compared to isotropic silica with the exception of the $\Omega = 90°$ orientation. In addition, the surface roughness of the Janus coatings and the imperfections at the Janus boundary found on some particles demonstrate the importance of understanding the behavior of particles that are the result of current fabrication processes as opposed to model homogenous or non-Janus particles. For Janus particles with a higher degree of amphiphilicity, adhesion force decreases as cap angle increases. A similar effect is seen for contact angle. As one increases the degree of amphiphilicity of the particle, the response is orientation dependent, where energetically unfavorable orientations show little difference in behavior with a change in wetting properties and energetically favorable orientations have an increase in contact angle and adhesion force with an increase in the degree of amphiphilicity.

AKNOWLEDGMENTS

This work was performed in part in the Materials Characterization and Fabrication Platform (MCFP) at the University of Melbourne. This research was in part supported by the National Science Foundation through the MRSEC program at the University of Chicago (DMR-1420709), the Air Force Office of Scientific Research (AFOSR # FA9550-14-1-0263), and PSC CUNY award 61783-00 49. EMK acknowledges the Corning Inc.'s Office of STEM Graduate Student Fellowship program for support.

References:

(1) Jiang, S.; Chen, Q.; Tripathy, M.; Luijten, E.; Schweizer, K. S.; Granick, S. Janus Particle Synthesis and Assembly. *Adv. Mater.* **2010**, *22* (10), 1060–1071. https://doi.org/10.1002/adma.200904094.

(2) Tu, F.; Lee, D. Shape-Changing and Amphiphilicity-Reversing Janus Particles with PH-Responsive Surfactant Properties. *J. Am. Chem. Soc.* **2014**, *136* (28), 9999–10006. https://doi.org/10.1021/ja503189r.

(3) Zhang, Y.; Chan, H. F.; Leong, K. W. Advanced Materials and Processing for Drug Delivery: The Past and the Future. *Adv. Drug Deliv. Rev.* **2013**, *65* (1), 104–120. https://doi.org/10.1016/J.ADDR.2012.10.003.

(4) Ebbens, S. J.; Howse, J. R. In Pursuit of Propulsion at the Nanoscale. *Soft Matter* **2010**, *6* (4), 726–738. https://doi.org/10.1039/B918598D.

(5) Faria, J.; Ruiz, M. P.; Resasco, D. E. Phase-Selective Catalysis in Emulsions Stabilized by Janus Silica-Nanoparticles. *Adv. Synth. Catal.* **2010**, *352* (14-15), 2359–2364. https://doi.org/10.1002/adsc.201000479.

(6) Prum, R. O.; Dufresne, E. R.; Quinn, T.; Waters, K. Development of Colour-Producing Beta-Keratin Nanostructures in Avian Feather Barbs. *J. R. Soc. Interface* **2009**, *6 Suppl 2* (Suppl 2), S253–S265. https://doi.org/10.1098/rsif.2008.0466.focus.

(7) Vukusic, P.; Sambles, J. R. Photonic Structures in Biology. *Nature* **2003**, *424* (6950), 852–855. https://doi.org/10.1038/nature01941.

(8) Forster, J. D.; Park, J.-G.; Mittal, M.; Noh, H.; Schreck, C. F.; O'Hern, C. S.; Cao, H.; Furst, E. M.; Dufresne, E. R. Assembly of Optical-Scale Dumbbells into Dense Photonic Crystals. *ACS Nano* **2011**, *5* (8), 6695–6700. https://doi.org/10.1021/nn202227f.

(9) Ding, H.; Zhu, C.; Tian, L.; Liu, C.; Fu, G.; Shang, L.; Gu, Z. Structural Color Patterns by Electrohydrodynamic Jet Printed Photonic Crystals. *ACS Appl. Mater. Interfaces* **2017**, *9* (13), 11933–11941. https://doi.org/10.1021/acsami.6b11409.

(10) Lotito, V.; Zambelli, T. Approaches to Self-Assembly of Colloidal Monolayers: A Guide for Nanotechnologists. *Adv. Colloid Interface Sci.* **2017**, *246*, 217–274. https://doi.org/10.1016/J.CIS.2017.04.003.

(11) Yuan, W.; Li, Q.; Zhou, N.; Zhang, S.; Ding, C.; Shi, L.; Zhang, K.-Q. Structural Color Fibers Directly Drawn from Colloidal Suspensions with Controllable Optical Properties. *ACS Appl. Mater. Interfaces* **2019**, *11* (21), 19388–19396. https://doi.org/10.1021/acsami.8b21070.

(12) Park, B. J.; Brugarolas, T.; Lee, D. Janus Particles at an Oil–Water Interface. *Soft Matter* **2011**, *7* (14), 6413–6417. https://doi.org/10.1039/C1SM05460K.

(13) Walther, A.; Müller, A. H. E. Janus Particles: Synthesis, Self-Assembly, Physical Properties, and Applications. *Chem. Rev.* **2013**, *113* (7), 5194–5261. https://doi.org/10.1021/cr300089t.

(14) Kumar, A.; Park, B. J.; Tu, F.; Lee, D. Amphiphilic Janus Particles at Fluid Interfaces. *Soft Matter* **2013**, *9* (29), 6604–6617. https://doi.org/10.1039/C3SM50239B.

(15) Razavi, S.; Koplik, J.; Kretzschmar, I. The Effect of Capillary Bridging on the Janus Particle Stability at the Interface of Two Immiscible Liquids. *Soft Matter* **2013**, *9* (18), 4585–4589. https://doi.org/10.1039/C3SM50210D.

(16) Razavi, S.; Koplik, J.; Kretzschmar, I. Molecular Dynamics Simulations: Insight into Molecular Phenomena at Interfaces. *Langmuir* **2014**, *30* (38), 11272–11283. https://doi.org/10.1021/la500376z.

(17) Lenis, J.; Razavi, S.; Cao, K. D.; Lin, B.; Lee, K. Y. C.; Tu, R. S.; Kretzschmar, I. Mechanical Stability of Polystyrene and Janus Particle Monolayers at the Air/Water Interface. *J. Am. Chem. Soc.* **2015**, *137* (49), 15370–15373. https://doi.org/10.1021/jacs.5b10183.

(18) Bradley, L. C.; Chen, W.-H.; Stebe, K. J.; Lee, D. Janus and Patchy Colloids at Fluid Interfaces. *Curr. Opin. Colloid Interface Sci.* **2017**, *30*, 25–33. https://doi.org/10.1016/J.COCIS.2017.05.001.

(19) Wei, P.; Luo, Q.; Edgehouse, K. J.; Hemmingsen, C. M.; Rodier, B. J.; Pentzer, E. B. 2D Particles at Fluid–Fluid Interfaces: Assembly and Templating of Hybrid Structures for Advanced Applications. *ACS Appl. Mater. Interfaces* **2018**, *10* (26), 21765–21781. https://doi.org/10.1021/acsami.8b07178.

(20) Binks, B. P. *; Fletcher*, P. D. I. Particles Adsorbed at the Oil–Water Interface: A Theoretical Comparison between Spheres of Uniform Wettability and “Janus” Particles. **2001**. https://doi.org/10.1021/LA0103315.

(21) Ondarçuhu, T.; Fabre, P.; Raphaël, E.; Veyssié, M. Specific Properties of Amphiphilic

Particles at Fluid Interfaces. *J. Phys. Fr.* **1990**, *51* (14), 1527–1536.

(22) Jiang, S.; Granick, S. Janus Balance of Amphiphilic Colloidal Particles. *J. Chem. Phys.* **2007**, *127* (16), 161102. https://doi.org/10.1063/1.2803420.

(23) Koplik, J.; Maldarelli, C. Molecular Dynamics Study of the Translation and Rotation of Amphiphilic Janus Nanoparticles at a Vapor-Liquid Surface. *Phys. Rev. Fluids* **2019**, *4* (4), 44201. https://doi.org/10.1103/PhysRevFluids.4.044201.

(24) Wang, X.; In, M.; Blanc, C.; Malgaretti, P.; Nobili, M.; Stocco, A. Wetting and Orientation of Catalytic Janus Colloids at the Surface of Water. *Faraday Discuss.* **2016**, *191* (0), 305–324. https://doi.org/10.1039/C6FD00025H.

(25) Adams, D. J.; Adams, S.; Melrose, J.; Weaver, A. C. Influence of Particle Surface Roughness on the Behaviour of Janus Particles at Interfaces. *Colloids Surfaces A Physicochem. Eng. Asp.* **2008**, *317* (1), 360–365. https://doi.org/https://doi.org/10.1016/j.colsurfa.2007.11.004.

(26) Kretzschmar, I.; Song, J. H. (Kevin). Surface-Anisotropic Spherical Colloids in Geometric and Field Confinement. *Curr. Opin. Colloid Interface Sci.* **2011**, *16* (2), 84–95. https://doi.org/https://doi.org/10.1016/j.cocis.2011.01.002.

(27) Ducker, W. A.; Senden, T. J.; Pashley, R. M. Measurement of Forces in Liquids Using a Force Microscope. *Langmuir* **1992**, *8* (7), 1831–1836. https://doi.org/10.1021/la00043a024.

(28) Ducker, W. A.; Xu, Z.; Israelachvili, J. N. Measurements of Hydrophobic and DLVO Forces in Bubble-Surface Interactions in Aqueous Solutions. *Langmuir* **1994**, *10* (9), 3279–3289.

https://doi.org/10.1021/la00021a061.

(29) Fielden, M. L.; Hayes, R. A.; Ralston, J. Surface and Capillary Forces Affecting Air Bubble–Particle Interactions in Aqueous Electrolyte. *Langmuir* **1996**, *12* (15), 3721–3727. https://doi.org/10.1021/la960145c.

(30) Preuss, M.; Butt, H.-J. Measuring the Contact Angle of Individual Colloidal Particles. *J. Colloid Interface Sci.* **1998**, *208* (2), 468–477. https://doi.org/10.1006/JCIS.1998.5833.

(31) Ecke, S.; Preuss, M.; Butt, H.-J. Microsphere Tensiometry to Measure Advancing and Receding Contact Angles on Individual Particles. *J. Adhes. Sci. Technol.* **1999**, *13* (10), 1181–1191. https://doi.org/10.1163/156856199X00866.

(32) Yakubov, G. E.; Vinogradova, O. I.; Butt, H.-J. Contact Angles on Hydrophobic Microparticles at Water–Air and Water–Hexadecane Interfaces. *J. Adhes. Sci. Technol.* **2000**, *14* (14), 1783–1799. https://doi.org/10.1163/156856100743239.

(33) Englert, A. H.; Krasowska, M.; Fornasiero, D.; Ralston, J.; Rubio, J. Interaction Force between an Air Bubble and a Hydrophilic Spherical Particle in Water, Measured by the Colloid Probe Technique. *Int. J. Miner. Process.* **2009**, *92* (3–4), 121–127. https://doi.org/10.1016/J.MINPRO.2009.03.003.

(34) Ally, J.; Kappl, M.; Butt, H.-J. Adhesion of Particles with Sharp Edges to Air–Liquid Interfaces. *Langmuir* **2012**, *28* (30), 11042–11047. https://doi.org/10.1021/la300539m.

(35) Zanini, M.; Lesov, I.; Marini, E.; Hsu, C.-P.; Marschelke, C.; Synytska, A.; Anachkov, S. E.; Isa, L. Detachment of Rough Colloids from Liquid–Liquid Interfaces. *Langmuir* **2018**,

34 (16), 4861–4873. https://doi.org/10.1021/acs.langmuir.8b00327.

(36) Rashidi, A.; Issa, M. W.; Martin, I. T.; Avishai, A.; Razavi, S.; Wirth, C. L. Local Measurement of Janus Particle Cap Thickness. *ACS Appl. Mater. Interfaces* **2018**, *10* (37), 30925–30929. https://doi.org/10.1021/acsami.8b11011.

(37) Prevo, B. G.; Velev, O. D. Controlled, Rapid Deposition of Structured Coatings from Micro- and Nanoparticle Suspensions. *Langmuir* **2004**, *20* (6), 2099–2107. https://doi.org/10.1021/la035295j.

(38) Neto, C.; Craig, V. S. J. Colloid Probe Characterization: Radius and Roughness Determination. *Langmuir* **2001**, *17* (7), 2097–2099. https://doi.org/10.1021/la001506y.

(39) Biggs, S.; Grieser, F. Atomic Force Microscopy Imaging of Thin Films Formed by Hydrophobing Reagents. *J. Colloid Interface Sci.* **1994**, *165* (2), 425–430. https://doi.org/10.1006/JCIS.1994.1246.

(40) Vakarelski, I. U.; Lee, J.; Dagastine, R. R.; Chan, D. Y. C.; Stevens, G. W.; Grieser, F. Bubble Colloidal AFM Probes Formed from Ultrasonically Generated Bubbles. *Langmuir* **2008**, *24* (3), 603–605. https://doi.org/10.1021/la7032059.

(41) Hutter, J. L.; Bechhoefer, J. Calibration of Atomic-force Microscope Tips. *Rev. Sci. Instrum.* **1993**, *64* (7), 1868–1873. https://doi.org/10.1063/1.1143970.

(42) Rezvantalab, H.; Shojaei-Zadeh, S. Capillary Interactions between Spherical Janus Particles at Liquid–Fluid Interfaces. *Soft Matter* **2013**, *9* (13), 3640–3650. https://doi.org/10.1039/C3SM27380F.

Effect of Orientation and Wetting Properties on the Behavior of Janus Particles at the Air-Water Interface

Ellen M. Knapp[1,2], Raymond R. Dagastine[2], Raymond S. Tu[1] and Ilona Kretzschmar[1*]*

[1] Department of Chemical Engineering, The City College of New York, New York, 10031, United States

[2] Department of Chemical Engineering and the Particulate Fluids Processing Centre, University of Melbourne, Parkville, 3010, Australia.

**Corresponding Authors: kretzschmar@ccny.cuny.edu, rrd@unimelb.edu.au*

Supporting Information

The supporting information presents additional representative force curve examples (unmodified (C0) Janus particles, C12 modified Janus particles, unmodified silica particle and C12 modified silica particle), He-Ion microcopy (HIM) images of probe particles without and with glue illustrating the stringent requirements applied during cantilever selection, and surface roughness characterization measurements for all cantilevers presented in the manuscript.

Figure S1 shows six examples of force curves obtained for (A) unmodified (C0) and (B) C12 modified Janus particle with gold hemisphere facing the bubble (Cantilever 1), (C) unmodified (C0) and (D) C12 modified Janus particle with silica hemisphere facing the bubble (Cantilever 10), (E) unmodified silica particle and (F) C12 modified silica particle. As in **Figure 1C** from the manuscript, the approach curve is red and the retract curve is blue. The scale of the curves illustrates the adhesion force; for example, for the case in which gold is facing the bubble there is a substantial increase in adhesion force with an increase in amphiphilicity (**Fig. S1A** versus **Fig. S1B**). Furthermore, the scale of curve **Figure S1B** is substantially larger than any other type of particle studied indicating strongest adhesion.

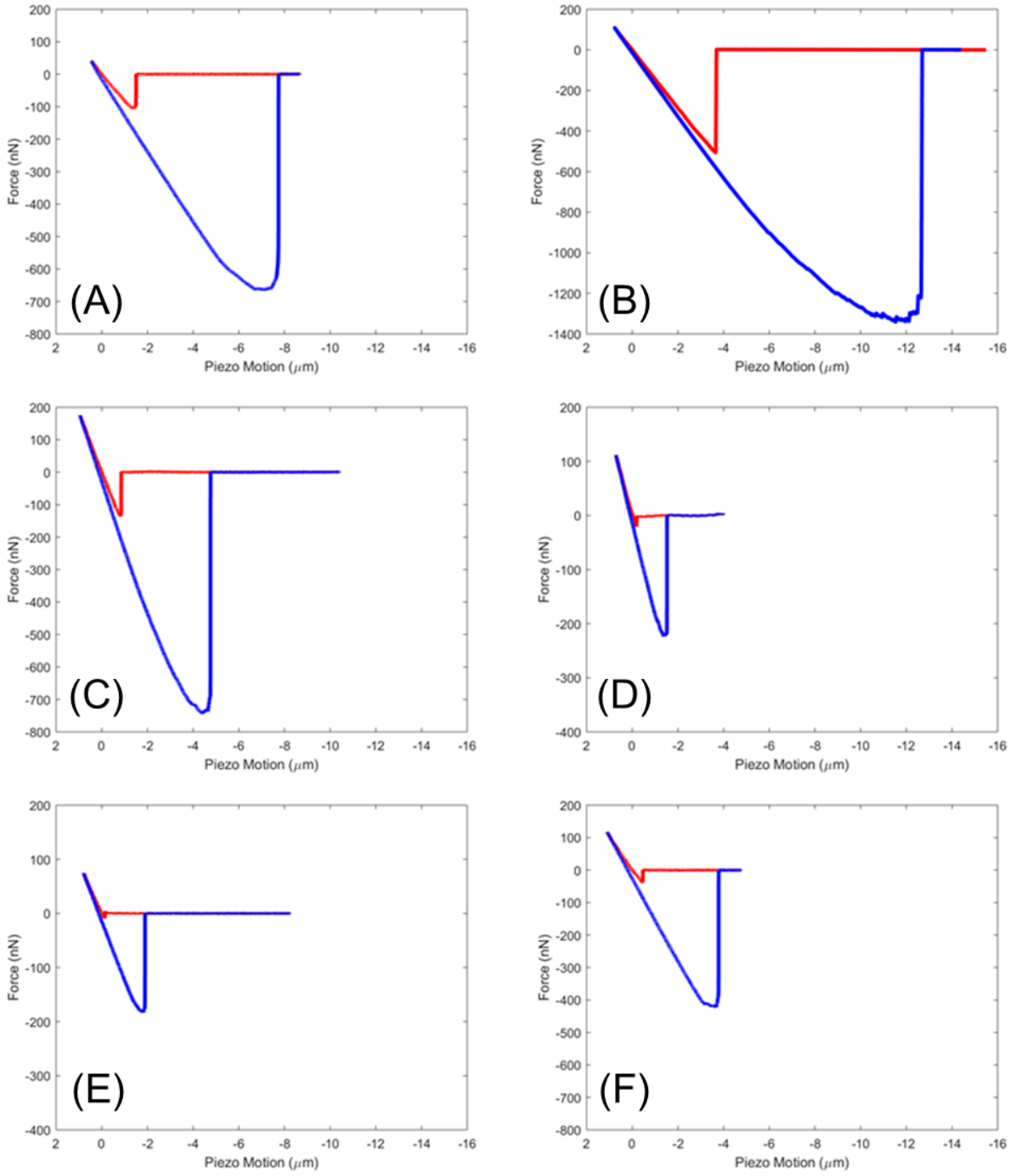

Figure S1: Example force curves for various particle types. (A) Unmodified (C0) Janus particle with its gold hemisphere facing the bubble (Cantilever 1). (B) C12 modified Janus particle with its gold hemisphere facing the bubble (Cantilever 1). (C) Unmodified Janus particle with its silica hemisphere facing the bubble (Cantilever 10). (D) C12 modified Janus particle with its silica hemisphere facing the bubble (Cantilever 10). (E) Unmodified silica particle (Silica 3). (F) C12 modified silica particle (Silica 3).

Figure S2 shows He-Ion microcopy (HIM) images of two Janus particles that are attached to cantilevers with the attachment procedure discussed in the manuscript. One of the particles (**Fig. S2** top: A-1 to A-4) shows a clear defect at the particle pole and also has excessive glue, which caused the elimination of data obtained from it from the overall analysis. The second particle (**Fig. S2** bottom B-1 to B-4), is an example of a Janus particle that passed inspection after the attachment procedure. The images show that there is clear particle-inherent surface roughness and Janus nature, but the glue is confined to the attachment area ensuring that the interfaces never interacts with the glue.

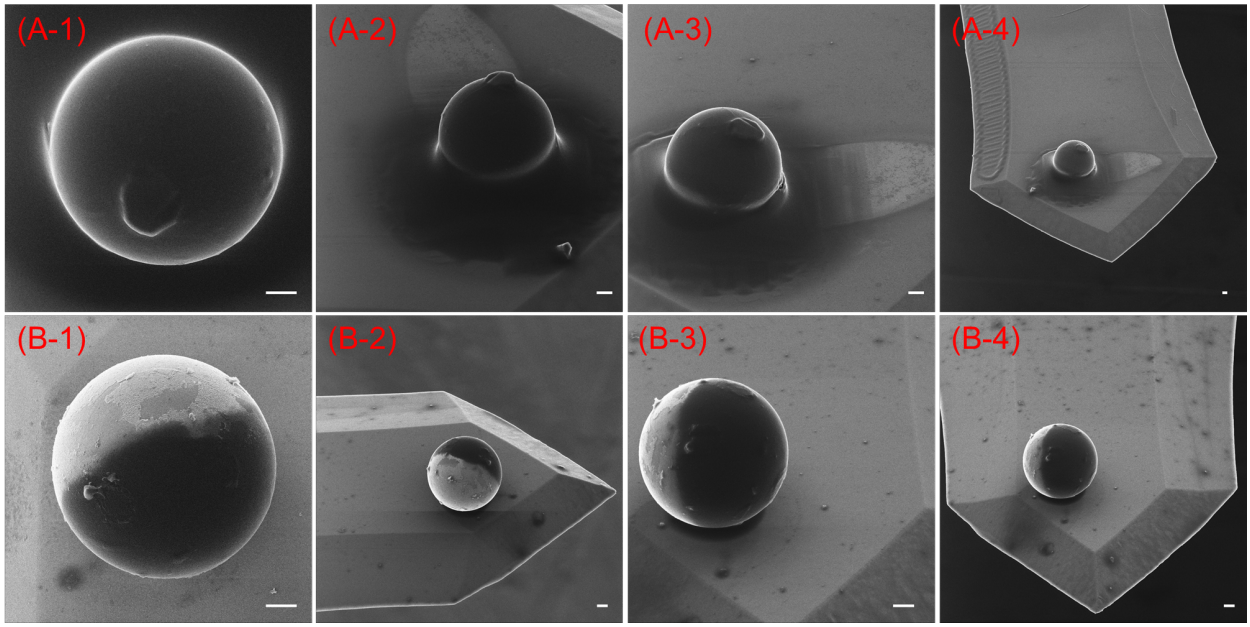

Figure S2: HIM images of Janus particles from various angles used to determine particles that are fit for analysis. (A) 1-4: Images of a Janus particle that was excluded from analysis due to excess glue. (B) 1-4: A Janus particle that was deemed acceptable for analysis (Cantilever 8). All scale bars are 1 μm.

Figure S3 shows a representative image obtained from reverse imaging of Cantilever 6 that is obtained using a spiked grating and the resulting root mean squared surface roughness obtained for the 12 cantilevers presented in the manuscript. Since the grating is a repeating pattern, multiple images of the particle are produced in **Figure 3SA**. Here, the cap defect can be seen in the lower left corner of the particle and is emphasized with a red arrow. The root mean squared surface roughness averages for various cantilevers shown in **Figure 3SB** vary from particle to particle within the range of 0.5 ± 0.1 nm (lowest RMS value, cantilever 7) to 7 ± 1 nm (highest RMS, cantilever 6). Averaging the surface roughness of cantilevers 1-5 and 9-silica 2, average root mean-squared surface roughness values of 1.1 ± 0.7 nm and 1.2 ± 0.8 nm are obtained for PVD-deposited gold and bare silica surfaces, respectively. The similarity of the two values indicates that the particle surface roughness is inherent to the SiO_2 base particles and not caused by the PVD-deposited gold film.

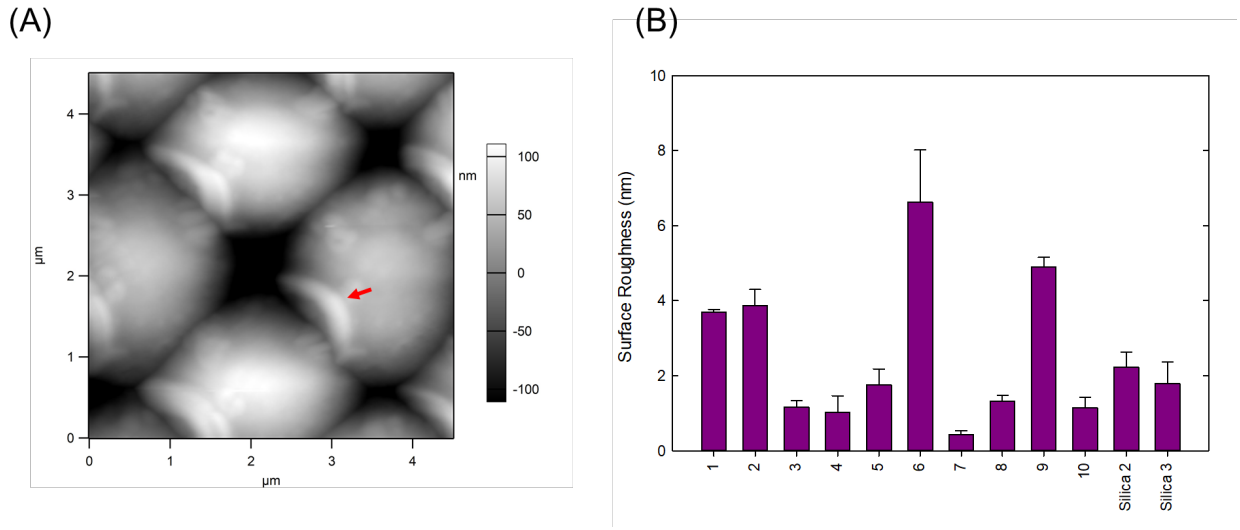

Figure S3: (A) Reverse imaging of Cantilever 6 done using a spiked grating. Red arrow indicates cap defect. (B) Root mean squared surface roughness averages for various cantilevers. Error bars represent one standard deviation.